Chemical Engineering Journal Advances 7 (2021) 100113

Contents lists available at ScienceDirect

Chemical Engineering Journal Advances

journal homepage: www.elsevier.com/locate/ceja

Development of marine oligosaccharides for potential wound healing biomaterials engineering

Hafez Jafari [a,*], Christine Delporte [b], Katrien V. Bernaerts [c], Gaël De Leener [d], Michel Luhmer [d,e], Lei Nie [f], Amin Shavandi [a,*]

[a] BioMatter-Biomass Transformation Lab (BTL), École polytechnique de Bruxelles, Université libre de Bruxelles (ULB), Avenue F.D. Roosevelt, 50, CP 165/61, 1050 Brussels, Belgium
[b] Laboratory of Pathophysiological and Nutritional Biochemistry, Faculty of Medicine, Université libre de Bruxelles (ULB), Route de Lennik, 808, CP611, 1070 Brussels, Belgium
[c] Maastricht University, Aachen-Maastricht Institute for Biobased Materials (AMIBM), Brightlands Chemelot campus, Urmonderbaan 22, 6167 RD Geleen, the Netherlands
[d] Centre d'Instrumentation en REsonance Magnétique – CIREM, Université libre de Bruxelles (ULB), Avenue F. D. Roosevelt 50, CP160/08, 1050 Brussels, Belgium
[e] Laboratoire de Résonance Magnétique Nucléaire Haute Résolution, Service de Chimie et PhysicoChimie Organiques, Université libre de Bruxelles (ULB), Avenue F. D. Roosevelt 50, CP160/08, 1050 Brussels, Belgium
[f] College of Life Sciences, Xinyang Normal University, Xinyang 464000, China

ARTICLE INFO

Keywords:
Chitooligosaccharide (CHOS)
Chitosan degradation
Microwave irradiation
Antioxidant activity
Antibacterial activity
Wound healing

ABSTRACT

This study aims to investigate the oxidative degradation of chitosan to produce chitooligosaccharides (CHOS) as a potential bioagent for biomaterials engineering. CHOS was produced *via* microwaved-assisted oxidative degradation of chitosan by using hydrogen peroxide in an acidic aqueous solution. The effects of the H_2O_2 concentration, reaction time, microwave power, and reaction temperature on the degradation of chitosan were investigated. Following optimization of these parameters, three soluble CHOS fractions CHOS 1 (4-8 kDa), CHOS 2 (3-5 kDa), and CHOS 3 (1-3 kDa) were synthesized and the physicochemical, structural, thermal properties and water solubility were investigated. No significant structure alteration of the initial chitosan was detected by Fourier transform infrared spectroscopy (FTIR), UV–vis, and nuclear magnetic resonance (NMR) analyses, making our microwave-assisted oxidative degradation a valuable method for the production of CHOS. Interestingly, CHOS fractions exhibited improved radical scavenging activities and antibacterial activities compared to the initial chitosan. The half maximal effective concentration (EC_{50}) of the CHOS fractions were found to be in the range of 2.69–0.724 mg/mL significantly lower than the chitosan (7.75, mg/mL). Besides, the CHOS fractions exhibited lower minimum inhibitory concentration (MIC; in the range of 62.5–500 μg/mL) compared to the initial chitosan (>1000 μg/mL). Moreover, the 3T3-Ll fibroblast cells treated with CHOS fractions exhibited more than 95% viability after 48 h of culture. Cell migration and collagen production assays also showed the positive effect of CHOS fractions, particularly CHOS 3. These results indicate that CHOS can be a promising bioactive agent in biomedical applications, in particular for wound healing applications.

1. Introduction

Patients with chronic wounds such as venous leg ulcers, pressure ulcers, or foot ulcers not only suffer from pain but also are exposed to the risk of severe infection and amputation [1]. There is an immense need for smart biomaterials to address the acute inflammation and antibiotic-resistant organisms in infected wounds [2]. Polysaccharides such as chitin, chitosan, alginate, and hyaluronic acid, have been widely used in the development of wound dressings due to their properties such as cytocompatibility, and biodegradability [3,4]. Chitosan with inherent antibacterial activity is one of the most cited polysaccharides for tissue engineering and drug delivery applications [5–7]. However, poor solubility of chitosan at natural pH and high swelling in acidic solution limits its biomedical applications [8].

Chitooligosaccharide (CHOS) is a depolymerized product of chitosan which comprises both 1,4-linked D-glucosamine (GlcN) and partially 1,4-linked N-acetyl-d-glucosamine (GlcNAc) units [9]. Although CHOS maintains the same chemical composition and structure as chitosan, it is water-soluble and exhibits biological activities such as antibacterial,

* Corresponding authors at: École polytechnique de Bruxelles, Université libre de Bruxelles (ULB), Avenue F.D. Roosevelt, 50, CP 165/61, 1050 Brussels, Belgium.
E-mail addresses: Hafez.Jafari@ulb.be (H. Jafari), nieleifu@yahoo.com (L. Nie), amin.shavandi@ulb.be (A. Shavandi).

https://doi.org/10.1016/j.ceja.2021.100113
Received 21 January 2021; Received in revised form 30 March 2021; Accepted 30 March 2021

antioxidant, anti-inflammatory activity, and wound healing potential compared to chitosan [10].

Different methods such as acid hydrolysis [11], gamma irradiation [12,13], oxidative degradation [14], and enzymatic hydrolysis [15] have been reported to produce CHOS from chitosan. Depending on the initial chitosan, and the degradation conditions, all of these methods lead to the production of CHOS with different molecular weights and degrees of acetylation and as a result, different physicochemical and biological properties [16].

Oxidative degradation of chitosan by H_2O_2 has been widely investigated due to its cost-effective process, high yield, and green chemistry without chemical residue and environmental issues [17]. However, the free radicals which are produced by H_2O_2 are not adequately efficient to convert chitosan to CHOS [17]. Several techniques such as gamma irradiation [18], plasma treatment [19], acid hydrolysis [20], enzymatic treatment [21], and chemical catalyst [22] can be combined with H_2O_2 to improve the chitosan degradation rate by increasing the concentration of radicals.

The microwave irradiation method is widely used in organic synthesis as a convenient source of heating with several advantages such as simple, clean, fast, efficient, and economic features for large-scale organic synthesis [23,24].

Although several studies reported the acceleration of chitosan oxidative degradation by using microwave irradiation assistance [14,25,26], the physiochemical properties of CHOS produced *via* oxidative degradation and its biological activities have not yet been reported. In the present work, the effect of hydrogen peroxide concentration, reaction time, microwave power, and reaction temperature on the microwave-assisted oxidative degradation of chitosan was studied. Then the physiochemical and biological activities of the obtained CHOS fractions with distinct average molecular weights were characterized. Two different viscometric techniques, rheometer on a chip, and rolling ball viscometers, were used to measure the molecular weight of CHOS. Physiochemical properties of CHOS such as chemical structure, degree of acetylation, crystallinity, and thermal properties were evaluated. In addition, biological activities of three CHOS fractions were monitored, including their antioxidant and antibacterial activities, their effects on cell viability, wound healing and collagen production.

2. Material and method

2.1. Materials and reagents

Chitosan from shrimp shells with a degree of deacetylation (DD) of a minimum of 75% was purchased from Sigma-Aldrich (St. Louis, MO, USA); DD was measured in the present study by ^{1}H NMR analysis and found to be about 90% (*vide infra*). Acetic acid (100%), hydrogen peroxide (H_2O_2) (30%), 3-(Trimethylsilyl)-1-propanesulfonic acid sodium salt (DSS) and Trypan blue powder were purchased from Merck Sigma-Aldrich (St Louis, MO, USA). Deuterium oxide (D_2O) and trifluoroacetic acid-*d* (CF_3COOD) were purchased from Eurisotop (Saint-Aubin, France). 3-(Trimethylsilyl)-1-propanesulfonic acid sodium salt (DSS) was purchased from Merck Sigma-Aldrich. Ethanol absolute (99% +) and Cell Tracker Blue CMAC (7-amino-4-Chloromethylcoumarin) were purchased from Thermo Fisher Scientific (Waltham, MA, USA). DPPH reagent was bought from Dojindo Laboratories (Kumamoto, Japan).

2.2. Microwave-assisted Chitooligosaccharide (CHOS) production

500 mg of chitosan powder was dissolved in 50 mL of 2% v/v acetic acid aqueous solution. H_2O_2 was added to this 1% wt chitosan solution and the mixture was treated by microwave irradiation under isothermal conditions (CEM Corporation Mars 5, Matthews, NC, USA). After microwave treatment, the reaction medium was cooled down to room temperature and neutralized by 5 M NaOH. Ethanol (250 mL) was then used to precipitate the sample. The light brown powder was collected by centrifugation at 4000 g for 10 min. Finally, the samples were freeze-dried at −80 °C for 24 h and stored at 4 °C. The effects of the H_2O_2 concentration (0.1, 0.3, 0.5, 1, 2, 3 and 4% v/v), maximum microwave power (400, 600, 800 and 1000 W), reaction temperature (50, 60, 70, 80, 90 and 100 °C) and reaction time (5, 10, 15, 20, 30, 40, 50, 60 and 70 min) were evaluated. In the following, the samples referred to as CHOS 1, CHOS 2 and CHOS 3 were obtained using 2% H_2O_2, 800 W, 80 °C and a reaction time of 5, 10, and 20 min, respectively.

2.3. Molecular weight determination of CHOS

The viscosity-average molecular weight of CHOS was determined by two different intrinsic viscosity determination methods, a rheometer on a chip viscometer and a rolling-ball viscometer. The viscosity-average molecular weight was calculated by the Mark-Houwink equation [27]:

$$[\eta] = K M^a \quad (1)$$

where k and a are Mark-Houwink constants, and for the buffer solution (0.2 M acetic acid/0.1 M sodium acetate) and chitosan system (degree of deacetylation 90%) at 25 °C are 6.589×10^{-3} and 0.88, respectively [27].

2.3.1. Intrinsic viscosity measurement with a rheometer on a chip viscometer

The measurements were performed with a m-VROC™ viscometer (RheoSense, San Ramon, CA) following previous reports [28, 29]. Freeze-dried samples were dissolved in 0.2 M acetic acid/0.1 M sodium acetate buffer with different concentrations (5–25 g/L). Measurements were performed in triplicate at 25 °C and viscosity was measured at five different concentrations (5–25 g/L) for a given molecular weight. Relative viscosity, $\eta_r = \eta/\eta_s$, was calculated from the measured solution viscosity η, and the solvent viscosity, η_s followed by specific viscosity ($\eta_{sp} = \eta_r - 1$). Intrinsic viscosity was calculated by linear extrapolation to zero concentration ($c = 0$) of reduced viscosity, $\eta_{red} = \eta_{sp}/c$, and inherent viscosity, $\eta_{inh} = \ln \eta_r/c$ following the Huggins equation.

2.3.2. Intrinsic viscosity measurement with a Rolling-ball viscometer

The measurements were performed using a Lovis 2000 M/ME Rolling-ball viscometer (Anton Paar GmbH, Germany) equipped with a glass capillary with a radius of 1.59 mm and a steel ball with a radius of 1.5 mm at an angle of 30°. Viscosity was measured at five concentrations (5–25 g/L) in the range of 5–25 g/L by plotting the measured reduced viscosity η_{red} against the polymer concentration and using the Huggins equation.

2.4. Physicochemical characterization of CHOS

^{1}H and ^{13}C NMR analyses of the native chitosan and CHOS fractions were performed at 25 °C using a JEOL JNM-ECZ600R/S3 spectrometer operating at 14.1 T (600.17 MHz for ^{1}H and 150.91 MHz for ^{13}C) equipped with a double resonance ROYAL™ probe. Samples were dissolved in 2% CF_3COOD/D_2O (v/v) at a concentration of 10 mg/mL for ^{1}H NMR and 50 mg/mL for ^{13}C NMR. The ^{1}H NMR spectra were recorded using a spectral width of about 20.0 ppm centred at 5.00 ppm, 4 s relaxation delay, 2.5 μs high-power RF pulse width (flip angle of 30°), 2.2 s acquisition time, and 256 scans. Proton-decoupled ^{13}C NMR spectra were recorded using a spectral width of about 250 ppm centred at 100.0 ppm, 3 s relaxation delay, 3.9 μs high-power RF pulse width (flip angle of 30°), 0.7 s acquisition time, 20,000 scans for the initial chitosan and 5000 scans for the CHOS fractions. Processing was performed using MestReNova 14.1.2–25024. It comprised zero-filling (total of 128k points), exponential apodization (line broadening factor lb = 1 Hz for ^{1}H and 2 Hz for ^{13}C) and Fourier transform of the free induction decay, followed by phase correction, baseline correction and

chemical shift referencing of the spectrum. The ^{1}H spectra were referenced to the trimethylsilyl signal of DSS ($\delta = 0.00$ ppm) using ethanol as secondary internal reference (δ $CH_3 = 1.17$ ppm). The ^{13}C spectra were referenced with respect to the CH_3 signal of ethanol (δ = 17.47 ppm) using CF_3COOD as secondary internal reference (δ CF_3 = 116.9 ppm) [30]. The degree of acetylation was determined by ^{1}H NMR using the following equation [31]:

$$DA\ (\%) = \left[\left(\frac{1}{3} \times I_{CH_3}\right) / \left(\frac{1}{6} \times I_{H2-H6}\right)\right] \times 100 \quad (2)$$

where I_{CH3} is the integral of the methyl signal of the *N*-acetyl-D-glucosamine units (H7 at 2.06 ppm, see Fig 3a) and $I_{H2\text{-}H6}$ stands for the total integral of the H2, H3, H4, H5 and H6 signals of both the acetylated and deacetylated units (region from about 3.0 to 4.5 ppm). The integral measurements were corrected for residual acetic acid and/or ethanol when necessary.

UV–vis spectra of samples were performed using a LAMBDA™ 25/35 Series UV/vis PerkinElmer spectrophotometer, in the range of 200–400 nm to investigate the effect of degradation parameters on the degradation of chitosan.

Fourier transform infrared spectroscopy (FT-IR; Bruker Vertex 70) was used to identify the functional groups of the CHOS fractions. The freeze-dried samples were mixed with KBr and pressed into a pellet for FTIR analysis over the region 400–4000 cm^{-1} with 32 scans referenced against air.

X-ray diffraction (XRD) patterns for investigating the distribution of the crystal structure in CHOS matrix were performed with an X-Ray Diffractometer (XRD; Bruker ecoD8 advance) in the range of $5^\circ<2\Theta<70^\circ$ with Cu Kα irradiation (k = 0.154060 nm) at 40 kV and 25 mhA. The scanning rate was 1.2°/min with a step size of 0.019 and scan step time of 96.00 s.

The thermal properties of chitosan and CHOS fractions were investigated by differential scanning calorimetric (DSC) and thermogravimetric analysis (TGA-DTA) analysis. TGA-DTA of samples was performed using a TA instrument (Netzsch STA 409 PC coupled with Netzsch QMS 403C). The samples (50 mg) were heated from 30 °C to 600 °C at 10 °C/min heating rate under nitrogen flow (60 mL/min). DSC was carried out using a Mettler Toledo DSC 821 in 30–400 °C in an inert nitrogen environment with a heating rate of 10 °C/min with an empty reference pan. The enthalpy (H in J/g dry weight), and onset (T_o), peak enthalpy (T_p), and end-set (T_e) temperatures, were measured automatically with TA 60 WS detector.

2.5. Water solubility

The water solubility of initial chitosan and CHOS fractions was evaluated by gross observation and turbidity assay according to a method previously described [32]. The pre-weighed samples were dissolved in deionized water at 10:1 (w/v) at pH 7.4. After 10 min of vortexing, the mixture was centrifuged at 10000 g for 10 min to check if the samples were dissolved. Furthermore, turbidity assay was used to determine the water solubility of the fractions over the pH range of 4–12. Briefly, samples (200 mg) were dissolved in 20 mL of acetic acid solution (1%) and the pH was adjusted to 4 by 1 mol/L NaOH. The light transmittance of the solution was determined by the stepwise addition of 0.1 mol/L NaOH, using the UV/vis spectrophotometer with an optical path length of 1 cm at 600 nm.

2.6. Antioxidant activity

The antioxidant activity of the chitosan and the CHOS fractions was investigated by DPPH (2,2-diphenyl-1-picryl-hydrazyl-hydrate) radical scavenging assay according to a previously reported method [33]. Briefly, 0.1 M DPPH solution was prepared in ethanol (99%) and mixed with the samples at various concentrations (0.1–10 mg/mL). The mixture was incubated at room temperature for 30 min, followed by measuring the absorbance at 517 nm. The radical scavenging activity was determined by using the following equation:

$$\text{Radical scavenging activity}\ (\%) = \left[1 - (A\_s/A\_c)\right] \times 100 \quad (3)$$

where A_s and A_C are the absorbances of the control (solvent: acetic acid 1%), and the absorbance of the sample, respectively. Besides, the EC_{50} of the samples was calculated by interpolation using linear regression analysis.

2.7. Antibacterial activity

Gram-negative bacteria including *Escherichia coli* ATCC 27195, *Pseudomonas aeruginosa* ATCC 15692, and *Serratia odorifera* and Gram-positive bacteria including *Staphylococcus aureus* ATCC 25923, *Staphylococcus epidermidis* ATCC 14990, and a yeast, *candida albicans* IHEM 3337 were chosen to study the antibacterial activity of CHOS fraction. A single-cell colony of freshly cultured bacteria was taken and inoculated in Muller–Hinton (M–H) broth. Bacteria suspensions in M–H broth were incubated at 37°C to obtain an absorbance value corresponding to 0.5 McFarland equivalent turbidity standard (10^8 CFU/mL). 10^6 CFU/mL bacteria suspensions were prepared as the inoculum. Sterile chitosan and CHOS fractions solutions (2 mg/mL) were prepared in M-H Broth medium by filtration using sterile 0.22 μm pore size membranes (Millipore Corporation, IL, USA) . Various concentrations of samples (2000–2 μg/mL) were tested by 2-fold serial dilution in 96 well plates, and the minimum inhibitory concentration (MIC) was determined *via* turbidity assay by measuring the absorbance at 620 nm after 24 h of incubation at 37 °C. All experiments were carried out in triplicates.

Furthermore, the disk diffusion method was used to evaluate the antibacterial activity of chitosan and CHOS fractions according to the method previously described [34]. 100 μL of bacterial cells (10^7 CFU/mL) were spread on Muller–Hinton agar plate. Then, a sterilized filter disk paper (0.4 cm) was located on the inoculated agar and treated with 60 μL of samples. The antibacterial activity was evaluated based on the diameter of the clear zone of growth inhabitation in comparison with the control (solvent: acetic acid 1%)

2.8. Cell culture

Fibroblasts 3T3-L1, received from Dr. I. Pirson [35] were grown in full culture media i.e., high glucose DMEM supplemented with 10% fetal calf serum (FCS), 200 U/mL penicillin, 200 U/mL streptomycin under a humidified atmosphere containing 5% CO_2.

2.9. Cell viability

The cell viability of 3T3-L1 was investigated by trypan blue assay based on a previously described method with some modification [36]. Briefly, 3T3-L1 cells were seeded at a density of 10^5 cell/well on 24 well plates and treated the next day with various concentrations (62.5–1000 μg/mL) of the initial chitosan and CHOS fractions. After 48 h of treatment, the cells were trypsinized and mixed with trypan blue dye (1:1). Cell viability was determined by measuring the number of live and dead cells by using a TC20 cell counter (BioRad, Hercules, CA, USA).

2.10. Wound healing assay

3T3-L1 cells were seeded at a cell density of 230,000 cells/well in a culture medium containing 10% FCS. using culture-insert 2 wells (Ibidi, Gräfelfing, Germany) with a defined cell-free gap (500 μm ± 50 μm) and well area of 0.22 cm^2. The next day, cells were incubated for 24 h with a culture medium containing 0.1% FCS. Then, cells were incubated for 60 min in a cell incubator with 10 μM of cell blue tracker (Thermofisher, Waltham, MA, USA) in a cell culture medium containing 0.1% FCS and washed 2 times with cell culture medium containing 0.1% FCS. Finally, the culture inserts were removed, and the cells were treated with cell culture media containing 0.1% FCS and in the absence

(control) or 1 mg/mL of each CHOS fractions. Three replicates were performed for each condition. Digital pictures were taken at 0, 24, and 48 h after removing the inserts. Images were analyzed to assess the width of the remaining cell-free gap

2.11. Collagen determination assay

3T3-L1 cells were seeded at a cell density of 2×10^5 cell/well in 6 well plates [37] and treated the next day for 72 h without (control) or with 1 mg/mL of initial chitosan or CHOS fractions. The content of soluble collagen in the cell supernatant was determined using a collagen assay kit (MAK322, Sigma Aldrich, St. Louis, MO, USA) as previously described [38]. In brief, 30 µL of master reaction mix containing assay buffer and digestion enzyme were mixed with 20 µL of samples and incubated for 1 h at 37 °C in black flat bottom 96 well plates. Then, 40 µL of dye reagent was added to all wells, following by incubation at 37 °C for 10 min. Finally, 8 µL of the developer reagent was added to all wells and incubated at 37 °C for 10 min. The fluorescence of the wells was read at $\lambda_{ex} = 375/\lambda_{em} = 465$ nm using a multimode microplate reader (Mithras Lb 940, Berthold Technologies, Bad Wildbad, Germany). A collagen standard curve (0–50 µg/ml range) was used for the determination of soluble collagen present in cell culture supernatant samples. All experiments were carried out in triplicate.

2.12. Statistical analysis

Values are expressed as means ± standard error of the mean (SEM). GraphPad Prism 8 (GraphPad Software Inc.) was used to perform statistical analyses by using two-way ANOVA followed by Bonferroni's post hoc test. *P*-values were calculated and $p < 0.05$ was considered statistically significant. Wherever significance has been proven, it is indicated by $^{*}p < 0.05$; $^{**}p < 0.005$; $^{***}p < 0.0005$; $^{****}p < 0.0001$.

3. Result and discussion

3.1. Synergistic degradation of chitosan by microwave irradiation and hydrogen peroxide

Oxidative degradation of chitosan by H_2O_2 is one of the most applicable approaches to obtained lower molecular weight chitosan [39]. The radical reaction has a prominent role in the oxidative degradation of chitosan. During this process hydrogen peroxide (H_2O_2) is decomposed to cationic hydrogen (H^+) and a perhydroxyl anion (HOO^-).

$$H_2O_2 = H^+ + HOO^- \quad (4)$$

$$H_2O_2 + HOO^- \rightarrow HO^{\bullet} + O_2{}^{-\bullet} + H_2O \quad (5)$$

The unstable perhydroxyl anion (HOO^-) reacts with H_2O_2 to form the highly reactive hydroxyl radical ($HO^{\bullet}$) and superoxide anion ($O_2{}^{-\bullet}$) that are powerful oxidants. These strong oxidants can attack the glycosidic bond of chitosan resulting in the scission of the chitosan chain and subsequently lowering the molecular weight of chitosan. The main degradation reaction of chitosan by the reaction with the hydroxyl radical ($HO^{\bullet}$) is attributed to the abstraction of carbon-bound hydrogen in the following equations:

$$(GlcN)_x - GlcN - O - GlcN - (GclN)_y + HO^{\bullet} \rightarrow (GlcN)_x - GlcN - O - {}^{\bullet}GlcN - (GlcN)_y + H_2O \quad (6)$$

$$(GlcN)_x - {}^{\bullet}GlcN - O - GlcN - (GclN)_y + H_2O \rightarrow (GlcN)_x + (GclN)_y \quad (7)$$

The strong hydroxyl radical ($HO^{\bullet}$) attacks the glycosidic bonds of chitosan and results in the scission of the glycosidic linkages to form chitooligosaccharides (CHOS) (Eqs. (6) and (7)).

Moreover, the degree of acetylation (AD) of chitosan can affect its oxidative degradation rate. Chitosan with more free amine groups (higher DD) is more susceptible to the reaction between NH_2 with H_2O_2 to break down the chitosan chain [17].

Microwave irradiation can assist the reaction through a dipolar polarization of polar particles and ionic conduction, which leads to heat generation and results in the acceleration of the chemical reaction [23]. Indeed, migration and rotation of particles-induced by microwave lead to the polarization of a particle, and the subsequent lag of this polarization and increasing the reversal field of the microwave results in friction among molecules and thus heat generation [40]. This heating is known as the "inside heating" due to the transition from the static to the dynamic state inside the molecule. Microwave irradiation can accelerate the chemical reactions up to 1240 times compared to traditional methods such as conventional heating [14].

Hence, the reaction activity of polar bonds can be increased through the absorption of microwave energy which accelerates the rate of breaking down of C–O–C glycosidic bond. It has been reported that oxidizing degradation of chitosan under microwave conditions had a significantly higher yield (reducing molecular weight) compared to conventional thermal degradation [26].

3.2. Effect of degradation parameters on chitosan degradation

3.2.1. Effect of H_2O_2 concentration on degradation

Various concentrations of H_2O_2 (0, 0.1, 0.3, 0.5, 1, 2, 3, 4%) were used to investigate their effects on the degradation of chitosan while the temperature, time, and microwave power were 80 °C, 20 min, and 800 W, respectively. Fig. 1a shows the effect of various H_2O_2 concentrations on the M_v of degraded chitosan. With increasing the concentration of H_2O_2 from 0.1% to 1%, the degradation rate of the chitosan increased and the samples' M_v decreased significantly from 6–11 kDa to 1–2 kDa.

However, a plateau was reached in the M_v with H_2O_2 concentration superior to 1%, which indicates that the presence of 1% H_2O_2 can produce enough radicals to degrade the chitosan. The result is consistent with the result reported by Li et al. [26]; however, the minimum H_2O_2 amount for reaching this plateau in the molecular weight depends on the source, the degree of acetylation of the initial chitosan, as well as the method of degradation. For example, Li et al. reported 0.3% H_2O_2 to reach the plateau for molecular weight by the microwave-assisted oxidative degradation of chitosan. However, in another study, Li et al. reported that increasing the H_2O_2 concentration to 3% consistently decreased the molecular weight of chitosan after degradation by conventional heating method [21] probably due to the lack of sufficient hydroxyl radicals compared to the microwave method indicating the beneficial effect of the microwave method in lowering the amount H_2O_2 for the same result.

Moreover, the degradation process of the chitosan by different concentrations of H_2O_2 was monitored by UV–vis spectrometry (Fig 1b). The UV spectra of samples indicated that the samples showed a broad peak between 250 and 280 nm after the degradation that was intensified with increasing H_2O_2 concentrations up to 1%. This could be due to the browning reaction during the degradation or generation of side reactions such as polysaccharide ring-opening, presence of aldehyde or carboxylic group [12,41]. However, H_2O_2 concentrations above 1% reduced the intensification of the peak, which is due to a prompt reduction in the darkness of hydrolysate due to the bleaching effect of H_2O_2 [21]. Although H_2O_2 concentrations superior to 2% could be desirable due to its bleaching effect, the removal of residual H_2O_2 could be challenging. Hence, a H_2O_2 concentration of 2% was chosen for CHOS production to avoid the browning reaction.

3.2.2. Effect of reaction time on degradation

The effect of different reaction times (5–70 min) on the degradation of chitosan was investigated using H_2O_2 concentration, temperature, and power of 1%, 80 °C, and 800 W during the microwave degradation, respectively.

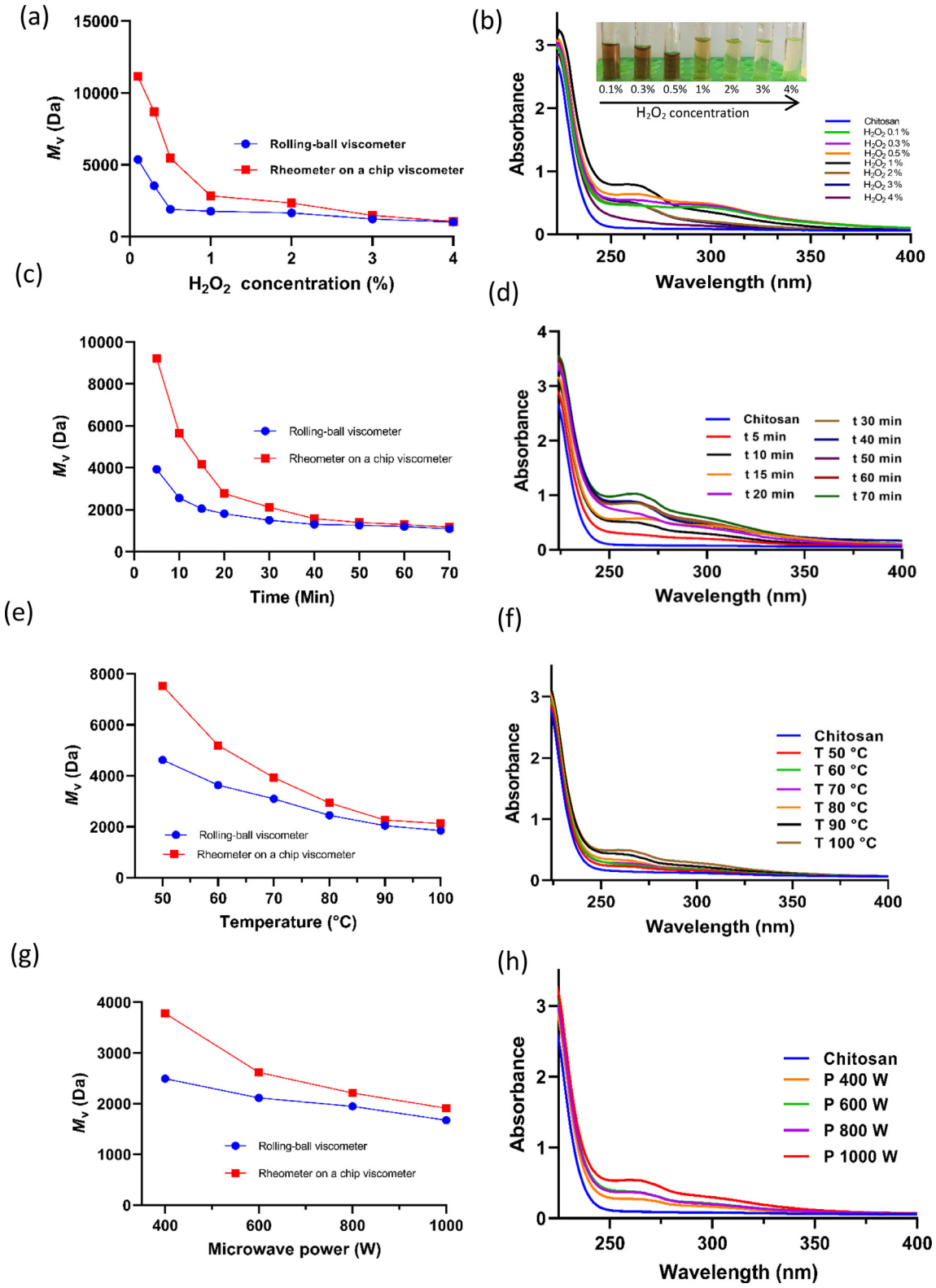

Fig. 1. (a) Effect of H_2O_2 concentration (%) on the viscosity average molecular weight of degraded chitosan, (b) UV–vis spectrometric scan of chitosan and degraded chitosan with different content of H_2O_2, (c) Effect of reaction time on the molecular weight of degraded chitosan, (d) UV–vis spectrometric scan of chitosan and degraded chitosan with different reaction times, (e) Effect of temperature on the molecular weight of degraded chitosan, (f) UV–vis spectrometric scan of chitosan and degraded chitosan with different degradation temperatures, (g) Effect of microwave power (W) on the molecular weight of degraded chitosan, (h) UV–vis spectrometric scan of chitosan and degraded chitosan with different microwave power (W).

Fig. 1c demonstrates the effect of time of degradation on the M_v of degraded chitosan. Increasing the reaction time from 5 to 70 min enhanced the degradation rate especially in the first 30 min and M_v decreased from 4–8 to 1–2 kDa. Indeed, increasing the reaction time up to 30 min significantly decreased the M_v of degraded chitosan to 2–3 kDa. However, continuing the process beyond 30 min did not have any significant effect in lowering the M_v.

Moreover, the effect of reaction time on the degradation process of chitosan was evaluated by UV–vis spectrometry (Fig 1d). The UV spectra of degraded chitosan with different reaction times showed that increasing the reaction time from 5 to 70 min intensified the peak between 250 and 280 nm, particularly after 20 min of degradation, indicating that further degradation of chitosan may lead to generating side reactions such as browning, ring-opening, and generation of carboxyl and aldehyde groups. However, up to 20 min degradation, there was not a significant difference in the UV spectrum with the initial chitosan. Hence, a lower reaction time inferior to 20 min is more favorable for CHOS production while maintaining the chemical structure of chitosan. Therefore, three different reaction times (5, 10, and 20 min) were chosen for CHOS production.

3.2.3. Effect of temperature on degradation of chitosan

The effect of different temperatures (50–100 °C) on the degradation of chitosan was investigated (Fig 1e and f) while other degradation parameters such as reaction time, H_2O_2 concentration, and microwave power were 20 min, 1%, and 800 W, respectively. Increasing the temperature from 50 to 100 °C, reduced the M_v of the degraded chitosan from 4–8 kDa to 2–3 kDa (Fig 1e).

Indeed, increasing the temperature from 50 to 100 °C enhanced the deprotonation of amino groups and the formation of oxidizing species, which leads to more degradation of chitosan [21,42]. However, a temperature above 80 °C induces a secondary reaction and intensifies the dark color of the hydrolysate, indicating the induction of a browning reaction. UV–vis spectra of the samples (Fig 1f) showed that increasing temperatures intensified a broad peak between 250 and 280 nm attributed to the browning reaction, which can be attributed to side reactions such as the ring-opening of polysaccharides ring and generating carboxylic acid and aldehyde groups in the later stage degradation of chitosan [43]. The broad peak occurring between 250 and 280 nm could be due to the presence of C=O bonds formed after the main chain scission of chitosan attributed to the ring-opening reaction [41]. However, the results revealed that there was no significant difference between the UV spectrum of the degraded and initial chitosan when the degradation temperature was below 80 °C. Therefore, 80 °C was used to produce CHOS fractions.

3.2.4. Effect of microwave power on the degradation of chitosan

The effect of microwave power on the M_v and chemical structure of chitosan after degradation was investigated (Fig. 1g and h). Different microwave powers (400, 600, 800, and 1000 W) were applied, while the temperature, time, and H_2O_2 concentration used were 80 °C, 20 min, and 1%, respectively.

Among the different degradation parameters such as time, temperature and H_2O_2 concentration, the microwave power showed a less reduction of the M_v of degraded chitosan. Given that pre-adjusted maximum microwave power was only constant until the samples reached the fixed temperature, then the power decreased to 10–15% of the adjusted power to keep the temperature constant. However, increasing the microwave power from 400 to 1000 W, slightly reduced the M_v from 2–4 kDa to 1–2 kDa. Moreover, like other parameters, increasing the microwave power intensified the peak between 250 and 280 nm indicating the increment of browning reactions (Fig 1h). Based on the M_v results and UV spectra, microwave power of 800 W was chosen for the CHOS fractions production.

3.3. Molecular weight determination

Viscosity average molecular weight (M_v) of CHOS was measured *via* calculating the intrinsic viscosity based on the Huggins equation [44], and subsequently using the Mark-Houwink equation to measure the M_v. Two different techniques were used to measure the intrinsic viscosity: a rheometer on a chip viscometer and a rolling-ball viscometer.

The M_v measured with a rheometer on a chip viscometer were two times higher compared to the results of the rolling-ball viscometer (Fig. 1a, c, e, and g). For example, the M_v at 5 min of degradation (Fig 1c) was 4 kDa measured with a rolling-ball viscometer and 9.2 kDa by a rheometer on a chip viscometer. This difference between the M_v is referred to as the difference in the measured intrinsic viscosity and probably could be due to different viscosity measurement principles of the rheometer on a chip viscometer and rolling-ball viscometer.

The viscosity measurement principle of rolling-ball viscometer is similar to the glass capillary viscometers, such as Ubbelohde and Ostwald viscometer, with the difference that it is possible to change the capillary tube angle enabling the viscometer to determine the viscosity of the solution with non-newton flow behavior like a chitosan solution. In a rolling-ball viscometer, a ball rolls through a liquid-filled capillary that is inclined at a defined angle. Three inductive sensors measure the ball's rolling time through liquids between defined marks and the liquid's viscosity is directly proportional to the rolling time.

The rheometer on a chip viscometer is a dynamic micro-sample viscometer that contains a measuring cell that reads the viscosity at a specific shear rate by measuring the pressure drop as a test liquid flows through its rectangular slit microfluidic channel. The rheometer on a chip viscometer measures the dynamic viscosity of the solvent and the polymer solution. The relative viscosity required for calculating intrinsic viscosity can be calculated through the proportion of solution viscosity to the solvent viscosity.

The dynamic viscosity of a polymer is influenced by its rheological behavior at different shear rates. Chitosan solution shows shear thinning behavior that can be affected by its concentration, molecular weight, ionic strength, and the temperature of the solution [45]. A chitosan solution with a higher concentration or a solution with higher molecular weights shows a different constant zero shear viscosity region as well as a different shear rate dependent apparent viscosity in comparison to a lower molecular weights chitosan solution. For example, Chao et al. reported a power-law relationship with chitosan concentration, and the zero shear viscosity region i.e. $\eta_0 \sim C^{4.1}$ [45]. Furthermore, Luo *et al.* investigated the rheological properties of four different chitosan with different molecular weights that ranged from 162 to 39 kDa [46]. The high molecular weights chitosan (162 kDa) showed a higher viscosity reduction with increasing the shear rate from 0.1 to 1000 1/s compared to lower molecular weight chitosan, indicating the effect of chitosan molecular weight, conformation, and structural flexibility on its apparent viscosity [47].

The difference between the M_v results derived from the intrinsic viscosity determination using a rheometer on a chip viscometer and a rolling-ball viscometer could be attributed to the molecular weight dependent shear thinning behavior of chitosan solution which can affect the viscosity results. Hence, rolling-ball viscometers with the ability to adjust the capillary angle are more favorable to measure the intrinsic viscosity of non-Newtonian fluids.

The M_v of CHOS 1, CHOS 2, and CHOS 3 (obtained following 5-, 10-, and 20-min reaction time) were 4.1, 2.85, and 1,65 kDa, respectively, measured by the rolling-ball viscometer. While, by using the rheometer on a chip viscometer, 8.46, 4.76, and 2.4 kDa were obtained for CHOS 1, CHOS 2, and CHOS 3 fractions, respectively. Based on M_v data obtained with both methods, the M_v range of CHOS 1, CHOS 2, and CHOS 3 were respectively 4–8 kDa, 3–5 kDa, and 1–3 kDa.

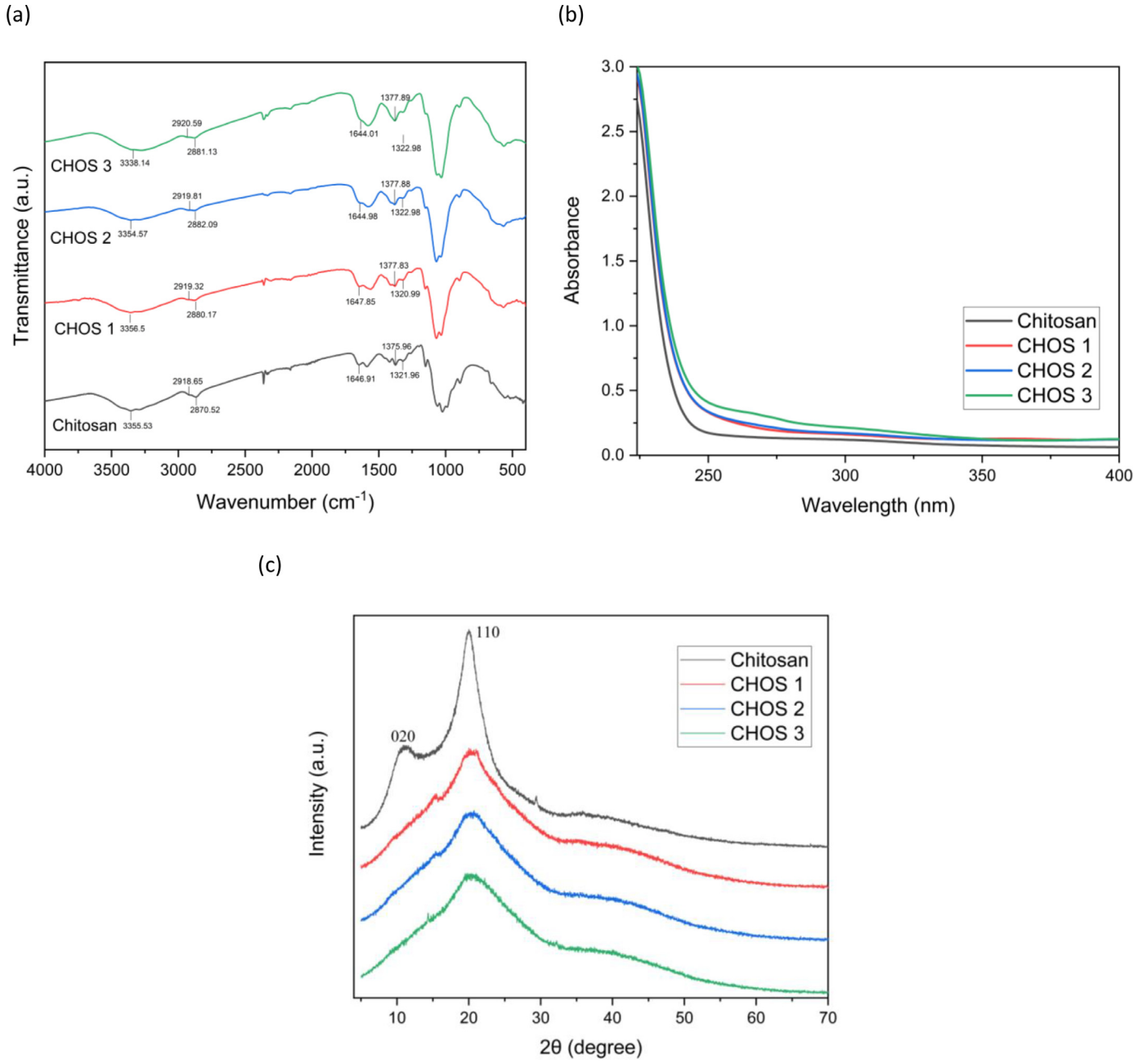

Fig. 2. Structural analysis of CHOS fractions with different molecular weights, CHOS 1 (4-8 kDa), CHOS 2 (3–5 kDa), CHOS 3 (1–3 kDa), (a) FTIR spectra of initial chitosan and CHOS fractions, (b) UV-vis spectra of initial chitosan and CHOS fractions, (c) X-ray diffraction pattern of initial chitosan and CHOS fractions.

3.4. FTIR and UV–vis analysis

FTIR spectra of the chitosan CHOS fractions exhibited a similar spectrum compared to the initial chitosan (Fig 2a), indicating that the main structure of the polymer has remained intact. A strong, broad peak centered around 3350–3400 cm^{-1} is assigned to both the N–H stretching and O–H stretching vibrations. Characteristic peaks at around 2920 and 2880 cm^{-1} are assigned to the C-H symmetric and asymmetric stretching, respectively which are characteristics typical of polysaccharides [48].

The peaks at around 1645 and 1320 cm^{-1} are attributed to the C=O stretching of amide I, and C-N stretching of amide III), respectively, which confirmed the presence of N-acetyl groups. Moreover, the characteristic peaks between 1158 and 895 cm^{-1} and a sharp peak at around 1378 cm^{-1} are attributed to the polysaccharide structure, and C–H bending and C–H stretching, respectively [49]. However, the appearance of new bands for carboxylic or aldehyde groups between 1650 and 1900 cm^{-1} in the CHOS spectra, cannot be observed reliably because of the presence of other peaks in this region, which might mask small peaks of the aldehyde or carboxylic side products. This means that further complementary analysis using i.e., NMR spectroscopy (see Section 3.6) is needed to conclude about the presence of aldehyde or carboxylic acid side products.

Furthermore, the UV–vis spectra of initial chitosan and CHOS fractions were investigated to check the λ_{max} changes (Fig 2b). Both chitosan and CHOS fractions exhibited a similar UV spectrum although an insignificant broad peak was observed around 250–280 nm for the CHOS fractions which can be due to the slight change in the color of the samples. FTIR and UV–vis results indicate that the microwave-assisted oxidative chitosan degradation does not lead to the ring-opening

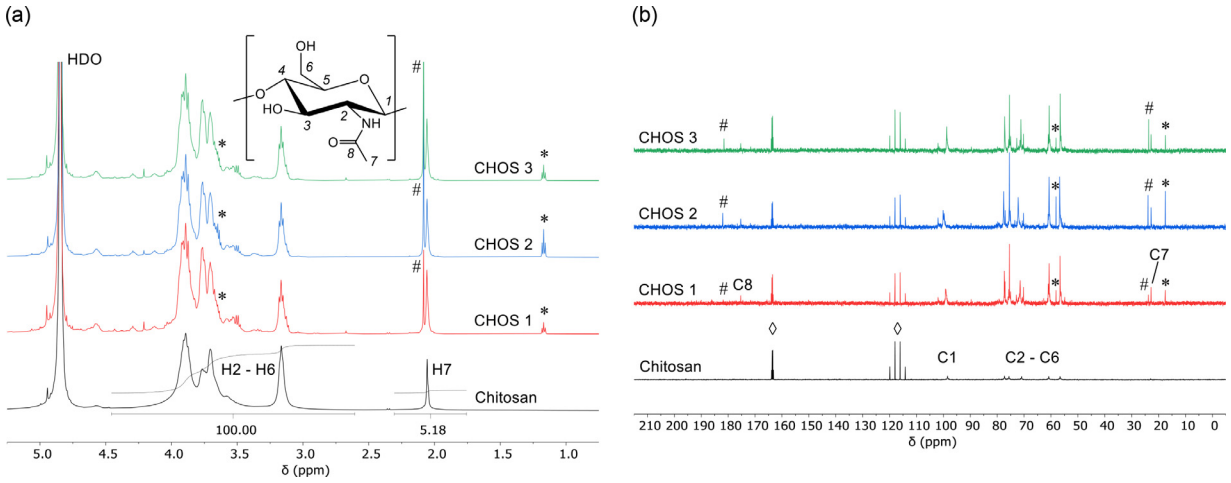

Fig. 3. (a) ^{1}H NMR spectra and (b) ^{13}C NMR spectra of chitosan and CHOS fractions. # Acetic acid, * ethanol, ◊ trifluoroacetic acid. Signal assignment is based on literature [21,52].

oxidation of glucosamine repeating units and the C–O–C glycosidic bond.

3.5. X-ray crystallography of the CHOS fractions

The X-ray diffraction patterns of initial chitosan and CHOS fractions are shown in Fig. 2c. The initial chitosan pattern demonstrated two characteristic peaks at $2\theta = 10.9^{\circ}$ and 20.11°, which are attributed to the (020) and (110) reflection [50]. The peak at (110) assigned to the I crystal form of chitosan, which is orthorhombic with a unit cell of $a = 7.76$ Å, $b = 10.91$ Å, and $c = 10.30$ Å, and (020) is attributed to II crystal form of chitosan [17]. After the degradation, the intensity of characteristic peaks at $2\theta = 20.11^{\circ}$ was lower than the chitosan, and the intensity was further decreased when the reaction time increased from 5 (CHOS 1) to 20 min (CHOS 3). The characteristic peak at $2\theta = 10.9^{\circ}$ completely disappeared for the CHOS fractions indicating the amorphous structure of CHOS. However, CHOS 1 showed a small peak at $2\theta = 15.29^{\circ}$ that could be due to the presence of the crystalline region because of the short time (5 min) of degradation.

During the degradation, first amorphous regions undergo depolymerization followed by the crystalline region [51]. In fact, in the crystalline region, first, the depolymerization was carried out at the surface of chitosan powder. After the depolymerization of the outer layer, the soluble layer is peeled off, and the depolymerization can proceed in the next layer [51]. Hence, first, the amorphous regions depolymerized and dissolved in water, and further depolymerization occurs in the crystalline parts leading to a decrease in the crystallinity. The depolymerization in the amorphous regions occurred by the penetrating pattern while the peeling-off pattern is responsible for the depolymerization crystal regions.

Hence, the presence of only a decreased peak at $2\theta = 20.11^{\circ}$ for the CHOS fractions, indicates further depolymerization of the crystalline regions of the CHOS fractions. Our result showed (Fig 2c) that microwave irradiation enhanced the degradation of chitosan so that even after 5 min of degradation, the crystalline regions of chitosan were completely depolymerized and resulted in water-soluble amorphous CHOS.

3.6. NMR analyses

^{1}H NMR and ^{13}C NMR analyses were performed to determine the degree of acetylation and investigate possible structural changes of chitosan following oxidative degradation. Compared to the spectrum of chitosan, the ^{1}H NMR signals of the CHOS fractions are less broadened, which is consistent with a lower average molecular weight (Fig 3a). Based on Eq. (2) the degree of deacetylation of chitosan was determined to be 89.6%. The corresponding DD values measured for the CHOS fractions are not significantly different (Table 2), indicating that the oxidative degradation of chitosan does not affect this structural parameter. The ^{13}C NMR signals of chitosan show extensive broadening and, consequently, the signals of the acetyl groups are below the detection limit (Fig 3b). Because of lower molecular weight of CHOS compared to the chitosan, the signals of the CHOS fractions are sharper and the acetyl signals are observed (C7 and C8). A similar ^{13}C NMR signature was obtained for the three CHOS fractions and no signal ascribable to aldehyde or carboxylic groups was detected. This strongly suggests that side reactions such as polysaccharide ring-opening are not significant, the skeleton of chitosan remaining unaffected [21].

3.7. Thermal properties

3.7.1. DSC analysis

The thermal properties of the initial chitosan and CHOS fractions were investigated by DSC and TGA analysis (Fig 4). DSC analysis exhibited two distinctive degradation steps for the chitosan and CHOS fractions (Fig 4a). In the chitosan and CHOS, the first and second endothermic peaks can be attributed to moisture loss and saccharide ring degradation, respectively [12].

The chitosan shows a lower temperature (≈ 117 °C) for the first endothermic peak a lower enthalpy (−101 J/g) compared to the CHOS fractions (≈130 °C, ≈200 J/g). Unlike the first degradation stage, the second degradation peaks of the CHOS fractions decreased to a lower temperature compared to the chitosan (from ≈ 310 °C to 290 °C), which could be due to the reduction in the molecular weight of the fractions. The results showed that the CHOS fractions exhibited a significant reduction in the energy for the phase transition temperature in comparison with the chitosan due to their lower molecular weight.

3.7.2. TGA analysis

Thermogravimetric analysis has been carried out to evaluate the thermal stability and degradation rate of chitosan and CHOS fractions (Fig 4b). Like DSC analysis, two stages of degradation were observed for the chitosan and CHOS fractions. The first weight loss occurred between 50 and 180 °C corresponding to the evaporation of moisture that existed in the samples. In the first degradation state, mass losses of the initial chitosan were around 9% while the CHOS fractions had a slightly increased mass loss between 12 and 13%.

The second degradation state was observed for all samples assigned to the decomposition of the saccharide structure, loss of water from the sugar ring, and degradation of both acetylated and deacetylated components. The chitosan exhibited the second decomposition state between

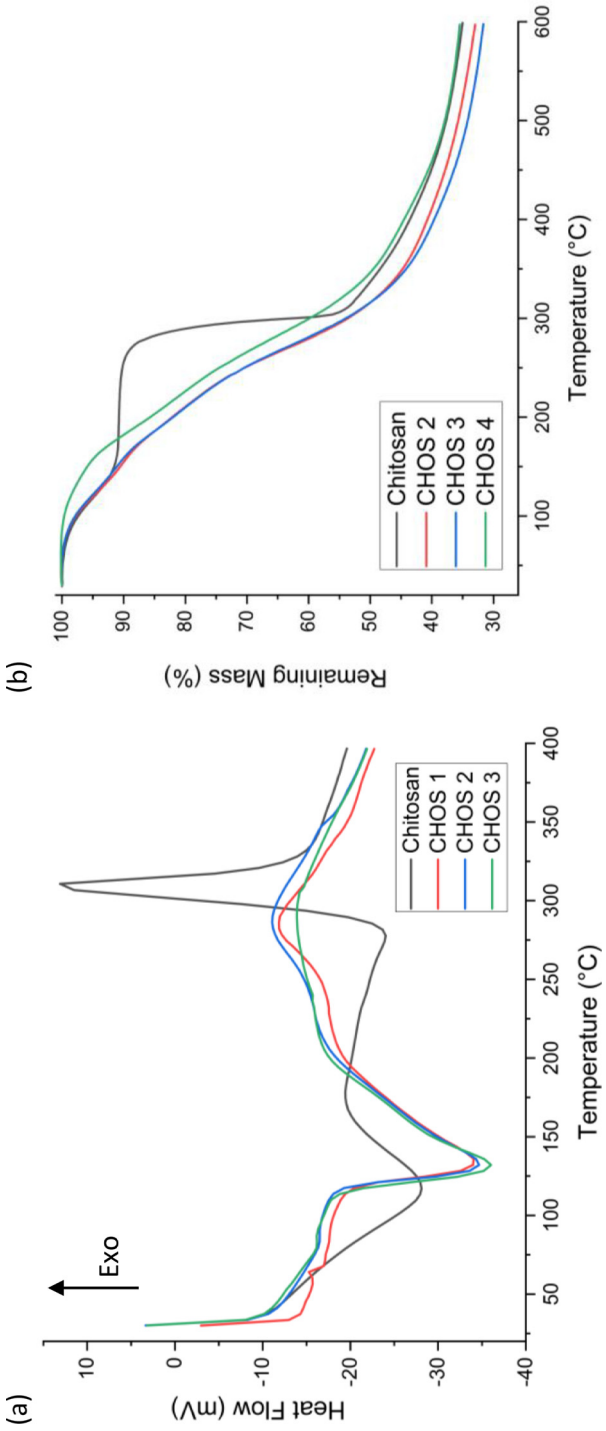

Fig. 4. (a) DSC thermograms in the 200–400 °C range of chitosan and CHOS fractions heated under a dynamic flow of nitrogen at the heating rate: 10 °C min^{-1}, (b) TGA curves of the chitosan and CHOS fractions heated from 30 to 600 °C at 10 °C min^{-1} under dynamic nitrogen atmosphere.

250 and 600 °C with a weight loss of 55%, while the second decomposition state for the CHOS fractions was observed continuously after the first degradation at 180–600 °C with a weight loss of around 55%. The remaining weights for all the samples were around 40% after 600 °C.

The results showed that the degradation process significantly decreased the thermal stability of the chitosan, indeed, the chitosan preserved its structure after the first degradation up to 250 °C (Fig 4b). However, the CHOS fractions showed a continuous degradation after the first degradation stage without a significant margin between two degradation states indicating the importance of molecular weight in the thermal stability of chitosan. Moreover, the maximum degradation temperatures (DTGmax) of the chitosan decreased from 309 to around 270 °C without any significant difference between the CHOS fractions which is aligned with the DSC results (Table 1).

The results demonstrated that CHOS fractions demonstrated lower thermal stability compared to the chitosan could be due to their lower molecular weight as well as weaker intermolecular chains interactions. The thermal stability of chitosan can be varied depending on the molecular weight, degree of acetylation, and source of chitosan [32,53].

3.8. Water solubility

The water solubility (gross observation) was determined based on the ability of the samples to dissolve in deionized water at a pH of 7.4 (at the concentration of 10 g/L). CHOS 2 and CHOS 3 fully solubilized after 5 min of mixing; however, CHOS 1 was dissolved after 2 h of mixing. Intermolecular and intramolecular hydrogen bonding of chitosan molecules plays a significant role in the formation of the crystalline regions and its water solubility. Increasing the degradation rate leads to lower molecular weights and subsequently less intermolecular and intramolecular hydrogen bonding and as a result less crystallinity which led to the high-water solubility of CHOS fractions. The water solubility of the samples indicated that the interaction between CHOS and water was higher than the interaction between the CHOS molecular chains.

Furthermore, a turbidity assay was performed to investigate the water solubility over the range of pH (4–12) (Fig 5a). The transmittance of initial chitosan started to decrease at pH 6.5 and suddenly dropped to 10.6% at pH 8. There was not any significant change in the transmittance of CHOS fractions over the full range of pH, and the solution was transparent without any precipitation even after 6 days at pH 12 indicating the high-water solubility of the samples (Fig 5b).

Various forces such as hydrophobic interactions, van der Waals forces, and prominently hydrogen bonding affect the water solubility of chitosan at the molecular level. In acidic media, the protonation of amino groups leads to the disruption of hydrogen bonds by forming electrostatic repulsion, and as a result, chitosan can be dissolved. Therefore, pH plays a major role in the solubility of chitosan due to its effect on the degree of charge of the units in polymer chains [54]. Indeed, at low pH (4) chitosan chains do not have a tendency for occupying a 2-fold helix structure which leads to a less strong hydrogen-bond network formation. However, increasing the pH causes a reduction in the degree of protonated amino groups, and therefore, higher hydrogen-bond interactions can lead to the predomination of the 2-fold helix structure which results in the precipitation of chitosan at around pH 6.5 [32].

Generally, precipitation due to the domination of hydrogen-bonding and also the formation of crystallites is the major parameter that causes a soluble-insoluble phase separation in chitosan. However, with decreasing the molecular weight, the chitosan chains do not tend to aggregate due to a reduction in the hydrogen-bonding and crystallinity according to the XRD results. Hence, depending on the degree of degradation and molecular weight, the soluble-insoluble transition can happen at higher pH (e.g., 8), or precipitation could not happen (our results) indicating the complete water solubility of CHOS.

Table 1
Thermal properties of the chitosan and the CHOS fractions.

Sample	TGA					DSC					
	First decomposition		Second decomposition		DTGmax (°C)	First decomposition (endothermic peak)			second decomposition (exothermic peak)		
	Mass Loss (%)	Temperature (°C)	Mass Loss (%)	Temperature (°C)		Onset (°C)	ΔH (J/g)	Peak (°C)	Onset (°C)	ΔH (J/g)	Peak (°C)
Chitosan	9.36	50–180	55.46	250–600	308	78	−100	117	293	169	309
CHOS 1	12.56	50–180	54.62	180–600	273	117	−187	134	255	79	283
CHOS 2	12.42	50–180	55.71	180–600	270	117	−210	132	243	69	287
CHOS 3	12.30	50–180	52.32	180–600	269	114	−195	131	286	32	291

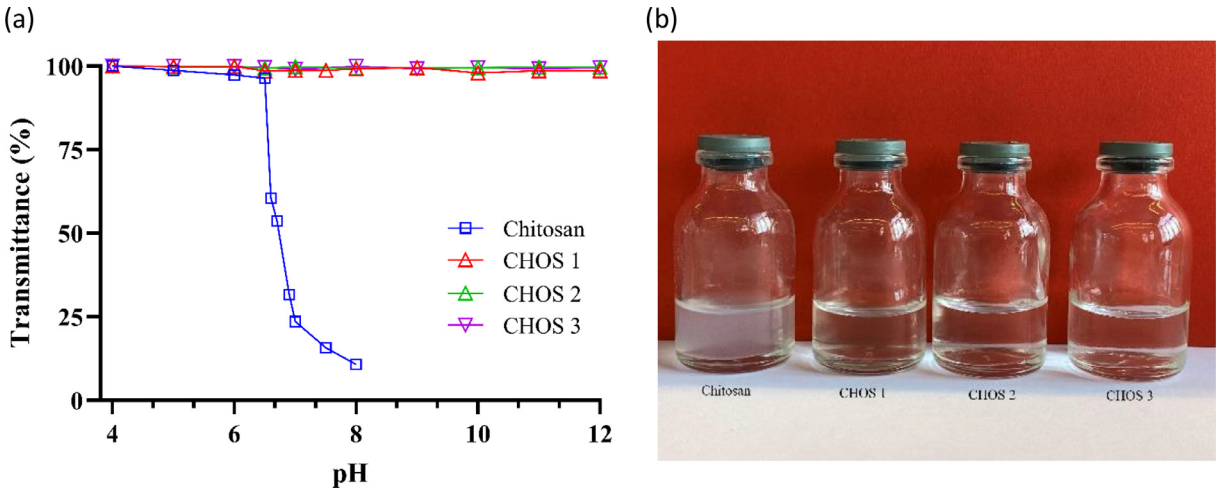

Fig. 5. The water solubility of initial chitosan and CHOS fractions, a) pH-dependent water solubility over the range of pH 4-12 at the concentration of 1 w/v%, b) water solubility of the initial chitosan and CHOS fractions at pH 12 after 6 days.

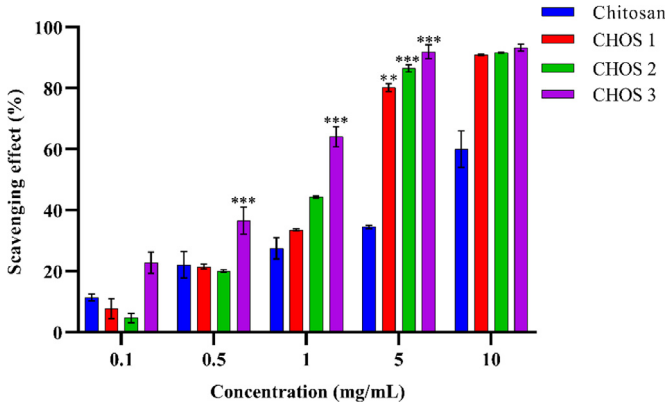

Fig. 6. DPPH radical scavenging effect of chitosan and CHOS fractions. Results are expressed as % of scavenging effect and are the mean ± SEM of three parallel measurements. Data were analyzed using two-way ANOVA, $p < 0.05$; $^{**}p < 0.005$; $^{***}p < 0.0005$; $^{****}p < 0.0001$ as compared to the chitosan.

3.9. Antioxidant activity

The scavenging activity against hydrogen radicals can be considered as one of the important mechanisms of antioxidation. DPPH scavenging activity of the chitosan and the CHOS fractions was concentration-dependent, within the range of 0.1–10 mg/mL concentration (Fig. 6).

The antioxidant activity of the chitosan was significantly lower compared to the CHOS fractions at the concentration of 5 mg/mL. The chitosan showed a 34.56 ± 0.8% scavenging effect, while the scavenging effect for the CHOS 1, CHOS 2, and CHOS 3 was 80.2 ± 1.7, 86.57 ± 1.6, and 91.94 ± 4.02%. Lower antioxidant activity of the chitosan compared to the CHOS fractions could be due to poor solubility and strong intermolecular and intramolecular hydrogen bonding of the chitosan.

The antioxidant activity of chitosan is due to the stable macromolecule radical formation as a result of the reaction between the hydroxyl groups (C6) and the amino groups (C2) with the hydroxyl and superoxide anion radicals [10]. Hence, higher intramolecular hydrogen bonding in the chitosan leads to a decrease in the number of available hydroxyl and free amine groups, and consequently a lower its antioxidant activity compared to CHOS [55].

The half-maximal effective concentration (EC_{50}) of the chitosan, CHOS 1, CHOS 2, and CHOS 3 were 7.75, 2.69, 2.14, and 0.724 mg/mL (Table 2), respectively indicating the significant difference in the antioxidant activity of CHOS and initial chitosan. Besides, it can be interpreted that decreasing *M*v of CHOS fractions from 4–8 kDa to 1–3 kDa, caused an improvement in the antioxidant acidity. According to the literature, the EC_{50} of CHOS was in the range of 0.22–3.24 mg/mL depends on the molecular weight, degree of acetylation, method production, and the source of initial chitosan [33,56–58].

In the samples with similar degree of acetylation (CHOS fractions), the difference in the antioxidant activity could be only due to the effect of molecular weight and intermolecular and intramolecular hydrogen bonding. Our result is aligned with the previous reports that by decreasing the molecular weight the antioxidant activity of the chitosan increases [57,59]. Our results showed that CHOS can be promising antioxidant agent in biomedical engineering, particularly in wound healing biomaterials.

3.10. Antibacterial activity

The antibacterial activity of chitosan and its derivatives is considered as one of its most important biological properties in which make it suit-

Table 2
Physiochemical and biological activity of the chitosan and the CHOS fractions.

Sample	Mv (kDa)	DA (%) [a]	DD(%) [a]	Water solubility [b]	EC_{50} [c](mg/mL)	MIC (μg/mL)					
						E. *coli*[d]	P. *aeruginosa*[e]	S. *aureus*[f]	S. *epidermidis*[g]	S. *odorifera*[h]	C. *albicans*[i]
Chitosan	50-190	10.4	89.6	Not soluble	7.75	1000	4000	2000	1000	1000	NA
CHOS 1	4-8	11.1	88.9	soluble	2.69	250	1000	500	250	125	NA
CHOS 2	3-5	11.2	88.8	soluble	2.14	250	500	500	250	125	NA
CHOS 3	1-3	11.4	88.6	soluble	0.724	125	500	250	62.5	32.25	NA

[a] The degrees of acetylation/deacetylation were calculated by ^{1}H NMR analysis.
[b] Water solubility was measured at the concatenation of 10 g/L in deionized water at pH 7.4.
[c] The half-maximal effective concentration in DPPH radical scavenging assay.
[d] Escherichia coli
[e] Pseudomonas aeruginosa
[f] Staphylococcus aureus
[g] Staphylococcus epidermidis
[h] Serratia odorifera
[i] Candida albicans

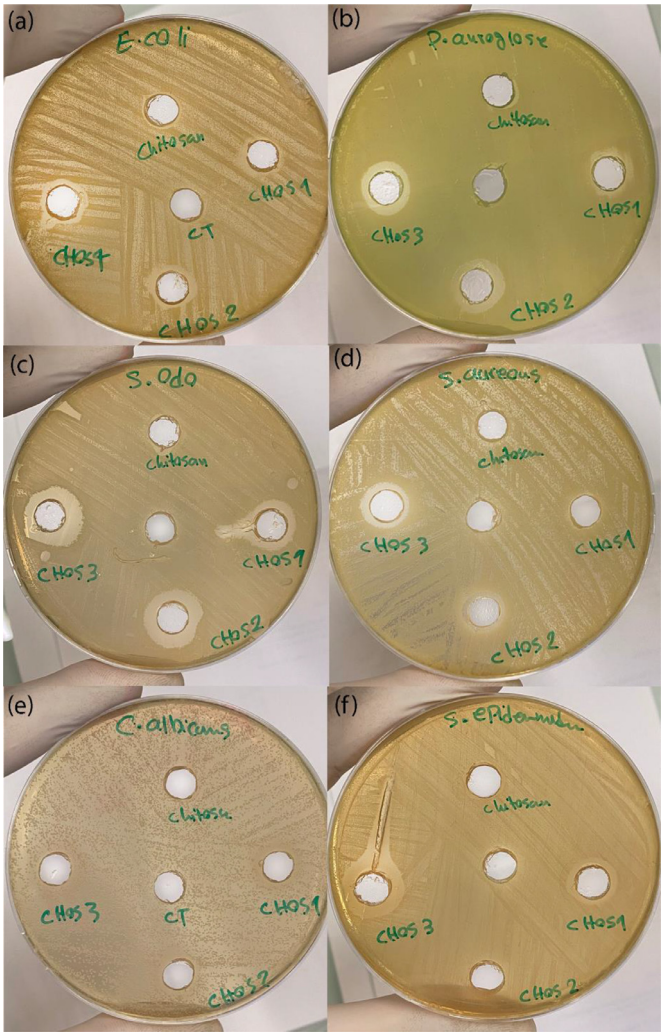

Fig. 7. Antibacterial activity of the chitosan and the CHOS fractions (10 mg/mL) against Escherichia coli (a), *Pseudomonas aeruginosa* (b), *Serratia odorifera* (c), *Staphylococcus aureus* (d), *Candida albicans* (e), and *Staphylococcus epidermidis* (f) by the disk diffusion assay.

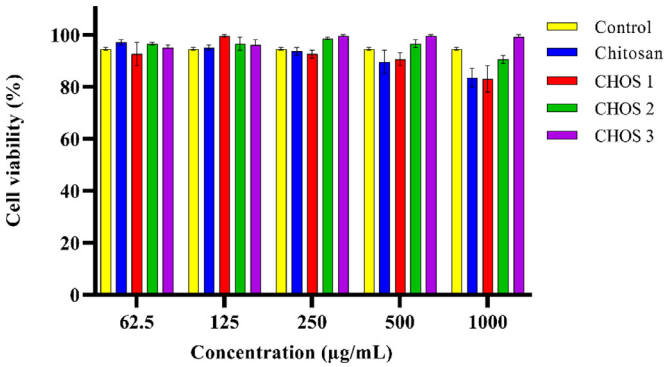

Fig. 8. Cell viability in response to chitosan and CHOS fractions treatment. 3T3-L1 cells were treated for 48 h in the absence or presence of increasing concentrations of the chitosan and the CHOS fractions (62.5, 125, 250, 500 and 1000 μg/mL). Results are expressed as % of cell viability and are the mean ± SEM of three independent experiments. Data were analyzed using two-way ANOVA test.

able for various applications such as food industry, tissue engineering, drug delivery and wound healing biomaterials [60]. Antibacterial activity of chitosan can be described by two mechanisms. The first mechanism is based on the cationic nature of chitosan which can interfere with bacterial metabolism by electrostatic stacking. Indeed, a polyelectrolyte complex between positively charged amine groups (C-2 position) and negatively charged carboxylic acid groups of bacterial cell surfaces leads to the formation of impermeable coating around the bacterial cell and results in the repression of bacterial metabolic activity and growth inhibition [10,61]. Besides, another mechanism is the penetration of chitosan into the DNA molecules and blocking of description to RNA from DNA, which required low molecular weight chitosan to penetrate the cell wall of the bacteria [61–63].

The minimum inhibitory activity (MIC) of chitosan and CHOS fractions were investigated toward various gram-positive and gram-negative bacteria as well as a yeast strain (Table 2). The CHOS fractions showed lower MIC in comparison with the chitosan toward the tested gram-positive and gram-negative bacteria indicating the stronger antibacterial activity of CHOS fractions (Table 2).

In the case of gram-negative bacteria, MIC of chitosan against E. *coli,* P. *aeruginosa, and S. odorifera* was 1000, 4000, and 1000 μg/mL, respectively, while CHOS fractions exhibited MIC of 500–125 μg/mL against E. *coli*, 1000–500 μg/mL against P. *aeruginosa,* and 125–32.25 μg/mL toward the *Serratia odorifera*. Similar to the gram-negative bacteria, CHOS fractions showed lower MIC against gram-positive strains, S. *aureus* and S. *epidermidis* Compared to the chitosan probably to due shorter polysaccharide chain results in easier cell wall entry (Table 2). Furthermore, CHOS fractions exhibited molecular weight dependent antibacterial activity against both S. *aureus* and S. *epidermidis* according to both MIC and inhibition zone test. Among CHOS fractions, CHOS 3 fraction showed the lowest MIC against S. *aureus* (250 μg/mL*)* and S. *epidermidis*

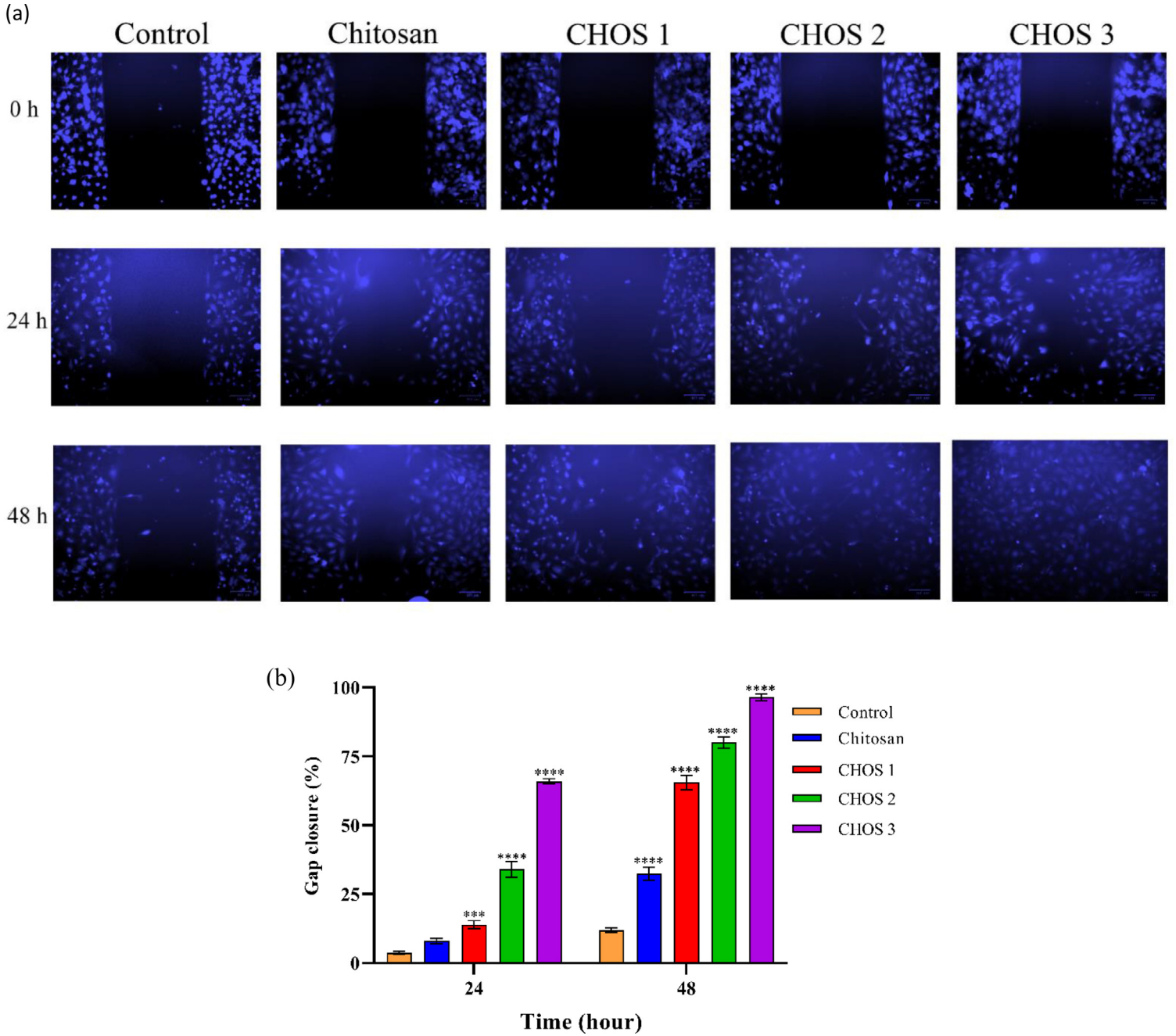

Fig. 9. a) Representative phase-contrast micrographs of *in vitro* cell migration assays of 3T3-L1 fibroblast cells treated with control (cell culture media), the chitosan, and the CHOS fractions at the concentration of 1 mg/mL. b) Quantification of the relative gap closure in the cell-free area of 3T3-L1 fibroblast cells treated with control, chitosan, and CHOS fractions. Results are expressed as % gap closure and are the mean ± SEM of three independent experiments. Data were analyzed using a two-way ANOVA test. $^{*}p < 0.05$; $^{**}p < 0.005$; $^{***}p < 0.0005$; $^{****}p < 0.0001$ as compared to the control.

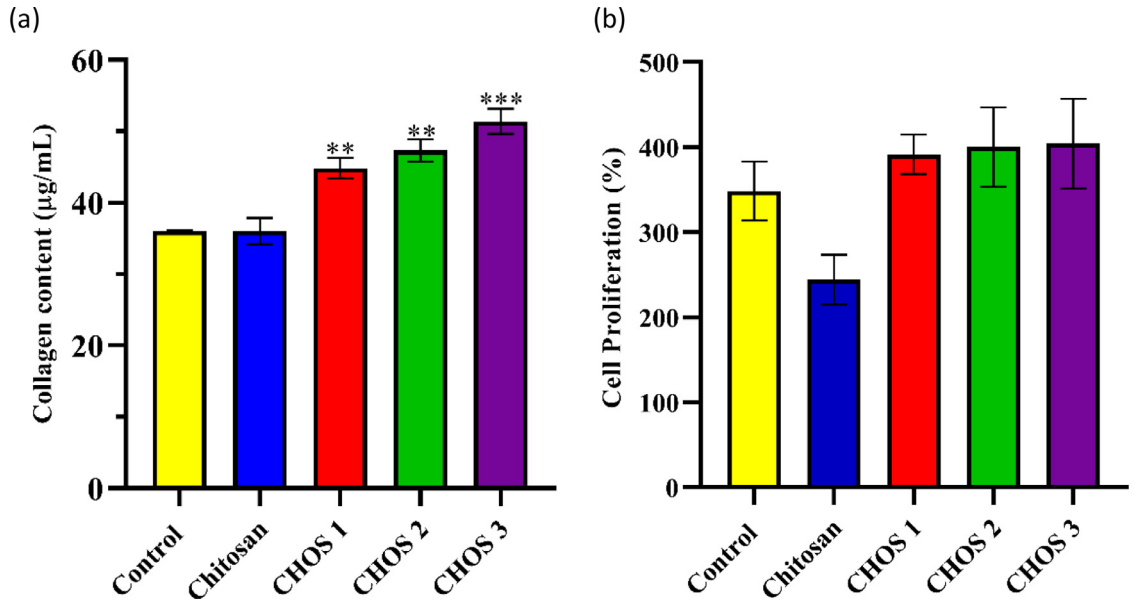

Fig. 10. Collagen production (a) and cell proliferation (b) in response to the chitosan and the CHOS fractions treatment. 3T3-L1 cells were treated for 72 h in the absence or presence of the chitosan and the CHOS fractions (1000 µg/mL). Results are expressed as the concentration of collagen produced by 3T3-L1 cells and the 3T3-L1 cells proliferation and are the mean ± SEM of three independent experiments. Data were analyzed using Two-way ANOVA test. $^{*}p < 0.05$; $^{**}p < 0.005$; $^{***}p < 0.0005$; as compared to control.

(62.5 µg/mL), indicating that decreasing molecular weight of CHOS enhanced its antibacterial activity against both gram-negative and positive bacteria. MIC results is aligned with disk diffusion test (Fig. 7). No inhibition zone was observed for chitosan against both gram-negative and -positive bacteria, while CHOS fractions, particularly CHOS 3 (1-3 kDa) significantly inhibited growth of both gram-negative and -positive bacteria probably to due shorter polysaccharide chain results in easier cell wall entry. However, no inhibition, and MIC was observed against C. *albicans* for both the chitosan and the CHOS fractions (Fig. 7e). Our results showed that CHOS fractions can be considered as a promising antibacterial agent, particularly for wound healing application due to their ability to prevent the growth of both gram-negative and -positive bacteria.

3.11. Cell viability

3T3-L1 fibroblasts were treated for 48 h in the absence or presence of increasing concentrations (62.5, 125, 250, 500, and 1000 µg/mL) of chitosan and CHOS fractions (Fig. 8). Chitosan and CHOS fractions had no significant effect on the cell viability at the concentrations used. Several studies have reported that CHOS increases the cell viability and proliferation of various cell lines, such as fibroblast, keratinocytes, and human umbilical vein endothelial cells (HUVECs), possibly due to its lower molecular weight and better water solubility than chitosan facilitating its cell entry [64–66]. These results showed that oxidative degradation of chitosan for CHOS production does not have any adverse effect on the cytocompatibility of chitosan.

3.12. Cell migration

Fibroblast and keratinocyte proliferation and migration play a major role in the proliferation phase wound healing process. Fibroblasts proliferation, and migration further induce keratinocyte proliferation and migration through keratinocyte growth factor (KGF), EGF, and fibronectin results in the acceleration of wound healing [67]. The effects of chitosan and CHOS fractions on 3T3-L1 cell migration was assessed using the wound healing assay (Fig. 9). After 24 h, the 3T3-L1 fibroblasts in all groups showed a tendency to migrate to close the scratch wound. All the CHOS fractions exhibited a significant difference compared to the control and around 40–70% of the gap was covered by the migrated cell. However, for the control, and chitosan groups, the closing gap was less than 25% (Fig 9b). Moreover, after 48 h, the cells were treated with chitosan and CHOS fraction revealed a higher migration (70–100%) of 3T3-L1 fibroblasts depending on the molecular weight in comparison with the chitosan (around 35%).

The result revealed that CHOS fractions can induce the migration of 3T3-L1 fibroblast cells, particularly, the cells treated with CHOS 3 (1–3 kDa) showed a complete migration and gap closure after 48 h. CHOS fractions showed a molecular weight dependent activity to induce cell migration; and by decreasing the Mv of CHOS from 4–8 to 1–3, the cell migration increased. This trend is similar to other biological activities of CHOS such as antioxidant, antibacterial and cell proliferation which [60,68]. Chen et al. reported that incorporation of CHOS into a porcine acellular dermal matrix (pADM) hydrogel enhanced the cell migration of L929 fibroblasts and human umbilical vein endothelial cells (HUVECs) [69].

3.13. Collagen content

The content of produced collagen by 3T3-L1 fibroblast treated with the chitosan and the CHOS fractions were determined using a collagen assay kit (Fig 10). The CHOS fractions exhibited a significantly higher collagen production compared to the chitosan and the control (culture media).

The collagen content of the control cells and cells treated with the chitosan, CHOS 1, CHOS 2 and CHOS 3 were 36 ± 0.2, 36 ±2.5,44.8 ± 2.02,47.3 ± 2.21 and 51.3 ± 2.5 µg/mL in the supernatant of cell culture media, respectively. Our results demonstrated that similar to other biological activities, chitosan has a molecular weight dependent collagen production activity. Decreasing the molecular weight of chitosan, brought about an increment in the collagen production activity which could be due to the shorter chain of CHOS compared to the chitosan which results in easier cell entry.

Moreover, the effects of chitosan and CHOS were also determined on the cell proliferation of 3T3-L1 fibroblasts treated for 3 days with the samples (Fig 10b). Cell proliferation decreased in the chitosan groups

compared to the control. 3T3-L1 fibroblasts treated by the CHOS fraction showed a higher cell proliferation (around 400%) compared to the chitosan (250%) and the control (350%) indicating that a greater number of cells in the CHOS fractions groups could produce a higher amount of collagen. Li *et al.* reported that CHOS can accelerate the wound healing process through increasing the proliferation of fibroblasts, and that collagen production results from the activation of the transforming growth factor-beta (TGF-β)-1-Smad2/3 pathway [70]. Another study indicated that CHOS was effective in the improvement of the thickness and integrity of epidermal tissue formation of collagen fibers [71]. Hence, CHOS can effectively accelerate wound healing process through the proliferation and migration of fibroblasts, and collagen synthesis by enhancing the re-epithelization [10,72].

4. Conclusion

Oxidative degradation of chitosan assisted by microwave irradiation was developed to produce chitooligosaccharides (CHOS). The effect of the degradation parameters such as time, temperature, H_2O_2 concentration, and microwave power on the molecular weight and chemical structure of degraded chitosan was investigated. Depolymerization of chitosan led to the production of lower molecular weight products alongside decreasing the crystallinity of the chitosan. Three water-soluble chitooligosaccharides (CHOS) fractions were produced and the physiochemical properties of the fractions were investigated. Chemical structural analysis by FTIR, UV-vis, and NMR spectroscopy indicated that CHOS fractions had a similar structure to the initial chitosan without generation of side reactions such as polysaccharide ring-opening reaction or production of carboxylic acid and aldehyde groups. Furthermore, the thermal analysis showed that the thermal stability of the chitosan was reduced due to the decrease in the molecular weight and its crystallinity. All CHOS fractions showed a full water solubility due to the reduction in the molecular weight which led to lower inter-and intramolecular hydrogen bonding, as well as lower crystallinity.

Besides, antioxidant activity measurement showed that the degradation of chitosan enhanced the DPPH radical scavenging activity from EC_{50} 7.75 mg/mL (initial chitosan) to 0.724 mg/mL (CHOS 3) indicating the molecular weight dependent biological activity of chitosan. Cell viability and migration, and collagen production assessment showed that the CHOS fractions exhibited a good cytocompatibility and positive effect on the migration of 3T3-L1 fibroblast, as well as enhanced collagen production which enables them to be used in biomedical applications particularly for wound healing applications.

Declaration of Competing Interest

The authors declare no conflict of interest.

CRediT authorship contribution statement

Hafez Jafari: Conceptualization, Methodology, Investigation, Validation, Formal analysis, Writing – original draft. **Christine Delporte:** Methodology, Validation, Writing – review & editing. **Katrien V. Bernaerts:** Methodology, Validation, Writing – review & editing. **Gaël De Leener:** Methodology, Investigation, Formal analysis, Writing – review & editing. **Michel Luhmer:** Methodology, Investigation, Formal analysis, Writing – review & editing. **Lei Nie:** Writing – review & editing. **Amin Shavandi:** Conceptualization, Methodology, Validation, Resources, Writing – review & editing, Project administration, Funding acquisition, Supervision.

Acknowledgments

H.J and A.S. acknowledge funding from Innoviris Brussels, Belgium (https://innoviris.brussels) under the project 2019 – BRIDGE – 4: RE4BRU. The content is solely the responsibility of the authors and does not necessarily represent the official views of the above-mentioned funding agency. The authors acknowledge Nargis Bolaky for her technical help with the cell studies. Besides, the authors acknowledge 4MAT research facilities and Ms. Tiriana Segato and Mr. Patrizio Madau for their help with XRD, FTIR, DSC and TGA measurements. We also acknowledge Dr. Véronique Fontaine for assiting withthe antibacterial test.

References

[1] G. Han, R. Ceilley, Chronic wound healing: a review of current management and treatments, Adv. Ther. 34 (3) (2017) 599–610.
[2] S. Das, A.B. Baker, Biomaterials and nanotherapeutics for enhancing skin wound healing, Front. Bioeng. Biotechnol. 4 (2016) 82.
[3] A. Abedi, M. Hasanzadeh, L. Tayebi, Conductive nanofibrous chitosan/PEDOT: PSS tissue engineering scaffolds, Mater. Chem. Phys. 237 (2019) 121882.
[4] T. Zhu, J. Mao, Y. Cheng, H. Liu, L. Lv, M. Ge, S. Li, J. Huang, Z. Chen, H. Li, Recent progress of polysaccharide-based hydrogel interfaces for wound healing and tissue engineering, Adv. Mater. Interfaces 6 (17) (2019) 1900761.
[5] A. Anitha, S. Sowmya, P.S. Kumar, S. Deepthi, K. Chennazhi, H. Ehrlich, M. Tsurkan, R. Jayakumar, Chitin and chitosan in selected biomedical applications, Prog. Polym. Sci. 39 (9) (2014) 1644–1667.
[6] A. Shavandi, A.E.-D.A. Bekhit, Z. Sun, A. Ali, M. Gould, A novel squid pen chitosan/hydroxyapatite/β-tricalcium phosphate composite for bone tissue engineering, Mater. Sci. Eng. 55 (2015) 373–383, doi:10.1016/j.msec.2015.05.029.
[7] A. Shavandi, A.E.-D.A. Bekhit, Z. Sun, M.A. Ali, Injectable gel from squid pen chitosan for bone tissue engineering applications, J. Sol-Gel Sci. Technol. 77 (3) (2016) 675–687, doi:10.1007/s10971-015-3899-6.
[8] D. Zhao, S. Yu, B. Sun, S. Gao, S. Guo, K. Zhao, Biomedical applications of chitosan and its derivative nanoparticles, Polymers 10 (4) (2018) 462.
[9] L. Phil, M. Naveed, I.S. Mohammad, L. Bo, D. Bin, Chitooligosaccharide: an evaluation of physicochemical and biological properties with the proposition for determination of thermal degradation products, Biomed. Pharmacother. 102 (2018) 438–451.
[10] H. Jafari, K.V. Bernaerts, G. Dodi, A. Shavandi, Chitooligosaccharides for wound healing biomaterials engineering, Mater. Sci. Eng. (2020) 111266.
[11] A. Il'Ina, V. Varlamov, Hydrolysis of chitosan in lactic acid, Appl. Biochem. Microbiol. 40 (3) (2004) 300–303.
[12] A.B. Muley, P.R. Shingote, A.P. Patil, S.G. Dalvi, P. Suprasanna, Gamma radiation degradation of chitosan for application in growth promotion and induction of stress tolerance in potato (Solanum tuberosum L.), Carbohydr. Polym. 210 (2019) 289–301.
[13] A. Shavandi, A.A. Bekhit, A.E.-D.A. Bekhit, Z. Sun, M.A. Ali, Preparation and characterisation of irradiated crab chitosan and New Zealand Arrow squid pen chitosan, Mater. Chem. Phys. 167 (2015) 295–302, doi:10.1016/j.matchemphys.2015.10.047.
[14] J. Shao, Y. Yang, Q. Zhong, Studies on preparation of oligoglucosamine by oxidative degradation under microwave irradiation, Polym. Degrad. Stab. 82 (3) (2003) 395–398.
[15] M. Pan, J. Li, X. Lv, G. Du, L. Liu, Molecular engineering of chitinase from Bacillus sp. DAU101 for enzymatic production of chitooligosaccharides, Enzyme Microb. Technol. 124 (2019) 54–62.
[16] B.B. Aam, E.B. Heggset, A.L. Norberg, M. Sørlie, K.M. Vårum, V.G. Eijsink, Production of chitooligosaccharides and their potential applications in medicine, Mar. Drugs 8 (5) (2010) 1482–1517.
[17] F. Tian, Y. Liu, K. Hu, B. Zhao, Study of the depolymerization behavior of chitosan by hydrogen peroxide, Carbohydr. Polym. 57 (1) (2004) 31–37.
[18] N.N. Duy, D. Van Phu, N.T. Anh, N.Q. Hien, Synergistic degradation to prepare oligochitosan by γ-irradiation of chitosan solution in the presence of hydrogen peroxide, Radiat. Phys. Chem. 80 (7) (2011) 848–853.
[19] C. Chokradjaroen, R. Rujiravanit, A. Watthanaphanit, S. Theeramunkong, N. Saito, K. Yamashita, R. Arakawa, Enhanced degradation of chitosan by applying plasma treatment in combination with oxidizing agents for potential use as an anticancer agent, Carbohydr. Polym. 167 (2017) 1–11.
[20] Z. Xia, S. Wu, J. Chen, Preparation of water soluble chitosan by hydrolysis using hydrogen peroxide, Int. J. Biol. Macromol. 59 (2013) 242–245.
[21] M. Li, J. Han, Y. Xue, Y. Dai, J. Liu, L. Gan, R. Xie, M. Long, Hydrogen peroxide pretreatment efficiently assisting enzymatic hydrolysis of chitosan at high concentration for chitooligosaccharides, Polym. Degrad. Stab. 164 (2019) 177–186.
[22] Z. Ma, Y. Wu, Y. He, T. Wu, A novel protocol for the oxidative degradation of chitosan with hydrogen peroxide catalyzed by peroxomolybdate in aqueous solution, RSC Adv. 3 (30) (2013) 12049–12051.
[23] S. Nain, R. Singh, S. Ravichandran, Importance of microwave heating in organic synthesis, Adv. J. Chem. Sect. A 2 (2) (2019) 94–104.
[24] A. Shavandi, A.E. Bekhit, Z. Sun, M.A. Ali, Bio-scaffolds produced from irradiated squid pen and crab chitosan with hydroxyapatite/β-tricalcium phosphate for bone-tissue engineering, Int. J. Biol. Macromol. 93 (Pt B) (2016) 1446–1456, doi:10.1016/j.ijbiomac.2016.04.046.
[25] T. Sun, D. Zhou, J. Xie, F. Mao, Preparation of chitosan oligomers and their antioxidant activity, Eur. Food Res. Technol. 225 (3–4) (2007) 451–456.
[26] K. Li, R. Xing, S. Liu, Y. Qin, X. Meng, P. Li, Microwave-assisted degradation of chitosan for a possible use in inhibiting crop pathogenic fungi, Int. J. Biol. Macromol. 51 (5) (2012) 767–773.
[27] W. Wang, S. Bo, S. Li, W. Qin, Determination of the Mark-Houwink equation for chitosans with different degrees of deacetylation, Int. J. Biol. Macromol. 13 (5) (1991) 281–285.

[28] A.O. Osaheni, P.T. Mather, M.M. Blum, Mechanics and tribology of a zwitterionic polymer blend: impact of molecular weight, Mater. Sci. Eng. 111 (2020) 110736.
[29] J. Zhang, M. Feng, X. Lu, C. Shi, X. Li, J. Xin, G. Yue, S. Zhang, Base-free preparation of low molecular weight chitin from crab shell, Carbohydr. Polym. 190 (2018) 148–155.
[30] G.R. Fulmer, A.J. Miller, N.H. Sherden, H.E. Gottlieb, A. Nudelman, B.M. Stoltz, J.E. Bercaw, K.I. Goldberg, NMR chemical shifts of trace impurities: common laboratory solvents, organics, and gases in deuterated solvents relevant to the organometallic chemist, Organometallics 29 (9) (2010) 2176–2179.
[31] A. Hirai, H. Odani, A. Nakajima, Determination of degree of deacetylation of chitosan by 1 H NMR spectroscopy, Polym. Bull. 26 (1) (1991) 87–94.
[32] M. Tian, H. Tan, H. Li, C. You, Molecular weight dependence of structure and properties of chitosan oligomers, RSC Adv. 5 (85) (2015) 69445–69452.
[33] T. Laokuldilok, T. Potivas, N. Kanha, S. Surawang, P. Seesuriyachan, S. Wangtueai, Y. Phimolsiripol, J.M. Regenstein, Physicochemical, antioxidant, and antimicrobial properties of chitooligosaccharides produced using three different enzyme treatments, Food Biosci. 18 (2017) 28–33.
[34] N. Rakkhumkaew, C. Pengsuk, Chitosan and chitooligosaccharides from shrimp shell waste: characterization, antimicrobial and shelf life extension in bread, Food Sci. Biotechnol. 27 (4) (2018) 1201–1208.
[35] C. Jacobs, S. Onnockx, I. Vandenbroere, I. Pirson, Endogenous SHIP2 does not localize in lipid rafts in 3T3-L1 adipocytes, FEBS Lett. 565 (1) (2004) 70–74, doi:10.1016/j.febslet.2004.03.076.
[36] D. Qi, M. Wang, F. Yu, Knockdown of lncRNA-H19 inhibits cell viability, migration and invasion while promotes apoptosis via microRNA-143/RUNX2 axis in retinoblastoma, Biomed. Pharmacother. 109 (2019) 798–805.
[37] C. Nicolaus, S. Junghanns, A. Hartmann, R. Murillo, M. Ganzera, I. Merfort, In vitro studies to evaluate the wound healing properties of Calendula officinalis extracts, J. Ethnopharmacol. 196 (2017) 94–103.
[38] Y. Inoue, H. Itoh, M. Aoki, S. Ogawa, T. Yamane, T. Baba, N. Tachibana, M. Kohno, Y. Oishi, K. Kobayashi-Hattori, Accelerating effect of soy peptides containing collagen peptides on type I and III collagen levels in rat skin, Biosci. Biotechnol. Biochem. 76 (8) (2012) 1549–1551.
[39] E. Purwanto, J. Connor, Y. Ngothai, The kinetics oxidative degradation of chitosan in formic acid with the presence of hydrogen peroxide, IOP Conference Series: Materials Science and Engineering, IOP Publishing, 2019.
[40] N. Haneishi, S. Tsubaki, E. Abe, M.M. Maitani, E.-i. Suzuki, S. Fujii, J. Fukushima, H. Takizawa, Y. Wada, Enhancement of fixed-bed flow reactions under microwave irradiation by local heating at the vicinal contact points of catalyst particles, Sci. Rep. 9 (1) (2019) 1–12.
[41] B. Kang, Y.-d. Dai, H.-q. Zhang, D. Chen, Synergetic degradation of chitosan with gamma radiation and hydrogen peroxide, Polym. Degrad. Stab. 92 (3) (2007) 359–362.
[42] C. Qin, Y. Du, L. Xiao, Effect of hydrogen peroxide treatment on the molecular weight and structure of chitosan, Polym. Degrad. Stab. 76 (2) (2002) 211–218.
[43] S.-M. Wang, Q.-Z. Huang, Q.-S. Wang, Study on the synergetic degradation of chitosan with ultraviolet light and hydrogen peroxide, Carbohydr. Res. 340 (6) (2005) 1143–1147.
[44] P.M. Reilly, B. Van Der Hoff, M. Ziogas, Statistical study of the application of the Huggins equation to measure intrinsic viscosity, J. Appl. Polym. Sci. 24 (10) (1979) 2087–2100.
[45] J. Cho, M.-C. Heuzey, A. Bégin, P.J. Carreau, Viscoelastic properties of chitosan solutions: Effect of concentration and ionic strength, J. Food Eng. 74 (4) (2006) 500–515.
[46] Q. Luo, Y. Wang, Q. Han, L. Ji, H. Zhang, Z. Fei, Y. Wang, Comparison of the physicochemical, rheological, and morphologic properties of chitosan from four insects, Carbohydr. Polym. 209 (2019) 266–275.
[47] S. Araki, T. Nakai, K. Hizume, K. Takeyasu, K. Yoshikawa, Hydrodynamic radius of circular DNA is larger than that of linear DNA, Chem. Phys. Lett. 418 (1-3) (2006) 255–259.
[48] M. Fernandes Queiroz, K.R.T. Melo, D.A. Sabry, G.L. Sassaki, H.A.O. Rocha, Does the use of chitosan contribute to oxalate kidney stone formation? Mar. Drugs 13 (1) (2015) 141–158.
[49] C. Branca, G. D'Angelo, C. Crupi, K. Khouzami, S. Rifici, G. Ruello, U. Wanderlingh, Role of the OH and NH vibrational groups in polysaccharide-nanocomposite interactions: A FTIR-ATR study on chitosan and chitosan/clay films, Polymer 99 (2016) 614–622.
[50] T.A.P. Hai, R. Sugimoto, Fluorescence control of chitin and chitosan fabricated via surface functionalization using direct oxidative polymerization, RSC Adv. 8 (13) (2018) 7005–7013.
[51] F. Tian, Y. Liu, K. Hu, B. Zhao, The depolymerization mechanism of chitosan by hydrogen peroxide, J. Mater. Sci. 38 (23) (2003) 4709–4712.
[52] M.R. Kasaai, Determination of the degree of N-acetylation for chitin and chitosan by various NMR spectroscopy techniques: a review, Carbohydr. Polym. 79 (4) (2010) 801–810.
[53] S. Mao, X. Shuai, F. Unger, M. Simon, D. Bi, T. Kissel, The depolymerization of chitosan: effects on physicochemical and biological properties, Int. J. Pharm. 281 (1–2) (2004) 45–54.
[54] M. Dash, F. Chiellini, R.M. Ottenbrite, E. Chiellini, Chitosan—a versatile semi-synthetic polymer in biomedical applications, Prog. Polym. Sci. 36 (8) (2011) 981–1014.
[55] F. Avelelas, A. Horta, L.F. Pinto, S. Cotrim Marques, P. Marques Nunes, R. Pedrosa, S.M. Leandro, Antifungal and antioxidant properties of chitosan polymers obtained from nontraditional Polybius henslowii sources, Mar. Drugs 17 (4) (2019) 239.
[56] H. Tomida, T. Fujii, N. Furutani, A. Michihara, T. Yasufuku, K. Akasaki, T. Maruyama, M. Otagiri, J.M. Gebicki, M. Anraku, Antioxidant properties of some different molecular weight chitosans, Carbohydr. Res. 344 (13) (2009) 1690–1696.
[57] J. Huang, D. Zhao, S. Hu, J. Mao, L. Mei, Biochemical activities of low molecular weight chitosans derived from squid pens, Carbohydr. Polym. 87 (3) (2012) 2231–2236.
[58] K. Li, R. Xing, S. Liu, R. Li, Y. Qin, X. Meng, P. Li, Separation of chito-oligomers with several degrees of polymerization and study of their antioxidant activity, Carbohydr. Polym. 88 (3) (2012) 896–903.
[59] S.T. El-Sayed, N.I. Omar, E.-S.M. El-Sayed, W.G. Shousha, Evaluation Antioxidant and cytotoxic activities of novel chitooligosaccharides prepared from chitosan via enzymatic hydrolysis and ultrafiltration, J. Appl. Pharm. Sci. 7 (11) (2017) 050–055.
[60] F. Liaqat, R. Eltem, Chitooligosaccharides and their biological activities: a comprehensive review, Carbohydr. Polym. 184 (2018) 243–259.
[61] J.Y. Kim, J.K. Lee, T.S. Lee, W.H. Park, Synthesis of chitooligosaccharide derivative with quaternary ammonium group and its antimicrobial activity against Streptococcus mutans, Int. J. Biol. Macromol. 32 (1–2) (2003) 23–27.
[62] Y. Yu, B. Tao, J. Sun, L. Liu, H. Zheng, Fabrication of chitosan-graft-polyaniline-based multilayers on Ti substrates for enhancing antibacterial property and improving osteogenic activity, Mater. Lett. (2020) 127420.
[63] D.F. Kendra, L.A. Hadwiger, Characterization of the smallest chitosan oligomer that is maximally antifungal toFusarium solani and elicits pisatin formation inPisum sativum, Exp. Mycol. 8 (3) (1984) 276–281.
[64] Y. Wang, Y. Zhao, C. Sun, W. Hu, J. Zhao, G. Li, L. Zhang, M. Liu, Y. Liu, F. Ding, Chitosan degradation products promote nerve regeneration by stimulating schwann cell proliferation via miR-27a/FOXO1 axis, Mol. Neurobiol. 53 (1) (2016) 28–39.
[65] P. Chandika, S.-C. Ko, G.-W. Oh, S.-Y. Heo, V.-T. Nguyen, Y.-J. Jeon, B. Lee, C.H. Jang, G. Kim, W.S. Park, Fish collagen/alginate/chitooligosaccharides integrated scaffold for skin tissue regeneration application, Int. J. Biol. Macromol. 81 (2015) 504–513.
[66] T. Minagawa, Y. Okamura, Y. Shigemasa, S. Minami, Y. Okamoto, Effects of molecular weight and deacetylation degree of chitin/chitosan on wound healing, Carbohydr. Polym. 67 (4) (2007) 640–644.
[67] S. Ellis, E.J. Lin, D. Tartar, Immunology of wound healing, Curr. Dermatol. Rep. 7 (4) (2018) 350–358.
[68] I. Hamed, F. Özogul, J.M. Regenstein, Industrial applications of crustacean by-products (chitin, chitosan, and chitooligosaccharides): a review, Trends Food Sci. Technol. 48 (2016) 40–50.
[69] Y. Chen, N. Dan, W. Dan, X. Liu, L. Cong, A novel antibacterial acellular porcine dermal matrix cross-linked with oxidized chitosan oligosaccharide and modified by in situ synthesis of silver nanoparticles for wound healing applications, Mater. Sci. Engineering: C 94 (2019) 1020–1036.
[70] A. Sionkowska, S. Skrzyński, K. Śmiechowski, A. Kołodziejczak, The review of versatile application of collagen, Polym. Adv. Technol. 28 (1) (2017) 4–9.
[71] X. Lv, Y. Liu, S. Song, C. Tong, X. Shi, Y. Zhao, J. Zhang, M. Hou, Influence of chitosan oligosaccharide on the gelling and wound healing properties of injectable hydrogels based on carboxymethyl chitosan/alginate polyelectrolyte complexes, Carbohydr. Polym. 205 (2019) 312–321.
[72] L. Van De Water, S. Varney, J.J. Tomasek, Mechanoregulation of the myofibroblast in wound contraction, scarring, and fibrosis: opportunities for new therapeutic intervention, Adv. Wound Care 2 (4) (2013) 122–141.